Intermittent Turbulence and Oscillations in the Stable Boundary Layer over Land. Part II: A System Dynamics Approach

B. J. H. VAN DE WIEL, A. F. MOENE, R. J. RONDA, H. A. R. DE BRUIN, AND A. A. M. HOLTSLAG

Department of Meteorology and Air Quality, Wageningen University, Wageningen, Netherlands

(Manuscript received 16 July 2001, in final form 11 January 2002)

ABSTRACT

In the stable boundary layer it is often observed that turbulence is not continuous in space and time. This discontinuous, intermittent turbulence causes alterations from the mean evolution of the stratified atmospheric boundary layer, which may result in an oscillatory type of behavior of the near-surface wind speed and temperature. This paper focuses on an intermittency generating mechanism that arises from a direct interaction of the lower atmosphere (first tens of meters) with the vegetation surface, without interaction with the air aloft. This atmosphere–surface intermittency (ASI) is associated with the essential elements of the stable boundary layer (SBL): strong surface cooling, the supply of mechanical energy by the synoptic pressure gradient, and the limiting effect of stratification on mixing efficiency. In Part I it is shown that the essence of ASI can be captured by a system of three coupled nonlinear differential equations. This simplified system shows both intermittent and nonintermittent flow regimes for different circumstances. In the present paper, this system is studied analytically, following a system dynamics approach. The transition between the different flow regimes is identified as a Hopf bifurcation. This property is used to derive a dimensionless parameter, which is a function of external parameters, such as radiative forcing and pressure gradient. With this dimensionless parameter the equilibrium behavior of the system (i.e., intermittent or nonintermittent) can be predicted exactly. As such this parameter is used to classify SBL regimes. It is shown that the proposed classification parameter provides different information about the state of the SBL than other typical SBL classification parameters such as z/L and Ri.

1. Introduction

On clear nights with weak winds, a frequently observed phenomenon is the weak and intermittent character of turbulence. Intermittent turbulence is characterized by brief episodes of turbulence with intervening periods of relatively weak or unmeasurable small fluctuations (Mahrt 1989, 1999). In this study we indicate intermittency by so-called global intermittency in a sense that in the periods of weak turbulence eddies on *all* scales are missing of suppressed. An observational example of this global intermittency is given in a companion paper by Van de Wiel et al. (2002, hereafter Part I). The discontinuous, intermittent turbulence causes changes in the mean evolution of the near-surface temperature and wind speed. In cases where the period of the intermittent turbulence is regular this may result in oscillatory behavior of the mean quantities. Therefore, in this text both ''oscillatory behavior'' and ''intermittency'' refer to the same phenomenon.

Intermittent turbulence can be generated by several physical mechanisms (see Part I). Traditionally, some of these mechanisms, like the formation and breaking of gravity waves, attracted a lot of attention, both from a theoretical and observational point of view (e.g., Hunt et al. 1985; Nappo 1991; Duynkerke 1991). In this paper we address another intermittency generating mechanism, which is generated by a direct atmosphere–surface interaction. This kind of intermittency is therefore referred to as atmosphere–surface intermittency (ASI; see Part I). The mechanism causing this ASI is a variation on the mechanism discussed qualitatively by Businger (1973) and Turner (1973). It is described as follows.

On clear nights thermal stability may increase quickly due to the strong cooling of the surface. As a consequence the gradient Richardson number increases considerably and therefore turbulence will be suppressed and will eventually collapse. This results in a decoupling of the air from the surface. Because of the very little friction acting on the air the omnipresent pressure force will start to accelerate the air mass. Thus, shear increases until $\mathrm{Ri} < \mathrm{Ri}_{\mathrm{crit}}$, eventually regenerating turbulence. As a result of this, turbulence shear is reduced quickly and soon thermal stability dominates over shear, the Richardson number increases, and turbulence is suppressed again. At this point the whole process will start over again. Several cycles of the behavior sketched above will result in an intermittent character of the turbulence

Corresponding author address: Dr. B. J. Van de Wiel, Department of Meteorology and Air Quality, Duivendaal 2, Wageningen University, Wageningen 6701 AP, Netherlands.
E-mail: Bas.vandeWiel@user.metair.wau.nl

in the near-surface stable boundary layer (SBL) and oscillations in the near-surface wind speed and temperature.

The above shows that the intermittency mechanism is closely related to the decoupling phenomenon (e.g., Derbyshire 1999), with the exception that in the intermittency case the SBL turbulence is able to ''recover'' by an increase of wind shear. An understanding of both phenomena is of great importance for numerical weather prediction (NWP) modeling, because decoupling in SBL models results in surface temperatures that are too low, compared to measured surface temperatures (Derbyshire 1999). In practice this problem is circumvented by application of empirical formulations parameterizing surface fluxes at high stabilities (e.g., Louis 1979; Holtslag and De Bruin 1988; Part I). However, these formulations are based on model performance rather than on surface-layer-based observations (Beljaars 1998). Therefore, prediction of decoupling and intermittency could be useful in future improvements of physically based surface-layer parameterization in NWP models.

At present it is not clear whether the intermittency mechanism described above generates intermittent turbulence aloft, for example, near the nocturnal jet [as studied by Vukelic and Cuxart (2000) and Ha and Mahrt (2001)], or that it generates intermittency near the surface via a direct atmosphere–surface interaction (e.g., Revelle 1993). In this study we confine ourselves to the direct atmosphere–surface interaction (first tens of meters), without considering interaction with the atmosphere aloft.

In Part I the results of SBL modeling studies by several authors are discussed. The models use first-order turbulence closure schemes (Blackadar 1979; Welch et al. 1986; Lin 1990; Revelle 1993; McNider et al. 1995). All these models show intermittent behavior of surface-layer turbulence for some parameter ranges, resulting in oscillating mean variables such as wind speed, temperature, and moisture. At present, however, a (quantitative) theoretical basis for this intermittency mechanism is still lacking. Thus, a better insight into this intermittency mechanism is needed. To this end, in Part I, the physical essentials of the models mentioned above are extracted, which results in a system of only three coupled nonlinear differential equations. The simplified model essentially shows the same behavior as the more complex models, resulting in intermittent and nonintermittent regimes for different parameter ranges.

The use of this simplified model enables us to study the complex interactions between the turbulent and radiative processes *analytically*, using a system dynamics approach. Our system dynamics approach is largely inspired by the work of McNider et al. (1995), who used numerical bifurcation techniques applied to a simplified model to study SBL dynamics. However, the latter authors did not explain the oscillatory behavior of the models mentioned above.

The two main goals of this paper are the following.

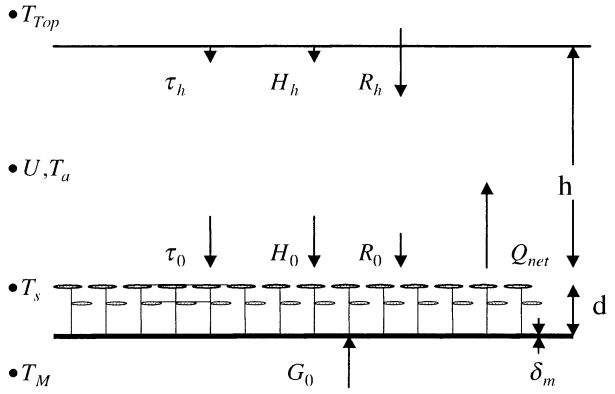

FIG. 1. An overview of the model system: state variables, fluxes, and model domain. The symbols are explained in appendix A. A detailed system description is given in Part I.

1) Provide a quantitative theoretical basis for the results of the numerical studies mentioned above. An exact stability criterion for intermittency will be given as a function of external forcing parameters. This gives the possibility to classify different SBL regimes into intermittent and nonintermittent cases.
2) Provide a further understanding of the instability mechanism causing intermittent behavior.

In section 2 the model equations derived in Part I are presented in their scaled form. In section 3 equilibrium solutions of the model are given and the formal stability criterion is derived. In section 4 a classification based on the criterion is introduced and compared with other classifications. For practical use, a simplified stability criterion and its physical interpretation are given in section 5. Discussion and conclusions are given in sections 6 and 7.

2. The system equations

In this text, point of departure is the set of equations given in appendix B, which is derived in detail in the companion paper (Part I). For the symbol list we refer to appendix A. This set of equations describes the time evolution of wind speed, air temperature, and surface temperature for a simple system consisting of four layers (Fig. 1).

- The soil, which is kept at a constant temperature T_M; $-\infty < z < 0$.
- The vegetation layer with depth d and surface temperature T_s (at canopy top); $0 \leq z \leq d$. Within this layer, at the bottom of the vegetation layer, a thin mulch/air layer with thickness δ_m is present, which has a negligible heat capacity but relatively low heat conductivity.
- The air layer, which has a constant depth h (the actual SBL); $d < z \leq h$.
- The ''free'' atmosphere above the SBL, with constant temperature; $h < z < \infty$.

As in Part I, this paper focuses on an intermittency generating mechanism that results from a *direct interaction of the lower atmosphere and the (vegetated) surface*. In this idealized case, interaction with the low-level jet and/or elevated turbulence [see review by Mahrt (1999)] is not considered. A discussion about the consequences of this idealization is given in Part I. Some other model characteristics include

- first-order closure of turbulence, with an exchange function depending on a bulk Richardson number;
- constant effective pressure force (i.e., component in the direction of the mean wind) imposed; Coriolis effects are neglected;
- constant boundary layer depth; and
- longwave radiation processes modeled using an emissivity approach.

For notational convenience, the equations given in appendix B will be scaled resulting in a compact set of equations. In our scaling analysis a few characteristic scales are needed: a timescale, a length scale, and a temperature scale. The boundary layer depth is taken as a characteristic length scale. The pressure force is used to define a velocity scale, because it drives the system. Note that, in our simplified system, the pressure gradient balances with the momentum flux divergence across the SBL, in stationary conditions. With the help of the characteristic length scale the velocity scale can be converted in a typical timescale. So we arrive at

$$\text{length scale } (h): \quad h;$$

$$\text{velocity scale } (U_k): \quad \left(-\frac{1}{\rho}\frac{\partial P}{\partial s}h\right)^{1/2};$$

$$\text{timescale } (\tau_{\text{bl}}): \quad \left(h \Big/ -\frac{1}{\rho}\frac{\partial P}{\partial s}\right)^{1/2}.$$

Next a characteristic temperature scale will be defined. The temperature difference between T_a and T_s will be driven mainly by the radiative cooling of the vegetation surface. In Part I it was shown that the isothermal net radiation, Q_i (Holtslag and De Bruin 1988), is a measure of the maximum cooling strength of the vegetation surface given the prescribed radiative conditions (ε_u, ε_s, and N). This Q_i will act upon the vegetation surface on a timescale τ_{bl}. For a vegetation layer with a total heat capacity per unit area of C_v (J m^{-2} K^{-1}) this will result in a typical temperature drop. Thus, a temperature scale is defined as

$$\text{temperature scale } (T_k): \quad \frac{|Q_i|\tau_{\text{bl}}}{C_v}.$$

The above-mentioned scaling parameters will be used to rewrite the equations of appendix B in their dimensionless equivalent. To this end we define the dimensionless wind speed $\hat{U}$, the dimensionless air $\hat{T}_a$, and soil $\hat{T}_s$ temperatures and time $\hat{t}$ by noting

$$\hat{U} = \frac{U}{U_k}; \qquad \hat{T}_a = \frac{T_a}{T_k}; \qquad \hat{T}_s = \frac{T_s}{T_k}; \qquad \hat{t} = \frac{t}{\tau_{\text{bl}}}.$$

Also, for notational convenience we define a radiative ''exchange coefficient'' as

$$a = 4\varepsilon_a \sigma T_{\text{ref}}^3,$$

and a neutral drag coefficient as

$$c_{Dn} = \kappa^2 \left[\ln\left(\frac{h/2}{z_0}\right)\right]^{-2}.$$

Substitution of the scaling variables $\hat{U}$, $\hat{T}_a$, $\hat{T}_s$, and $\hat{t}$ in the original set in appendix B gives

$$\frac{\partial \hat{U}}{\partial \hat{t}} = 1 - c_{Dn}\hat{U}^2 f(\hat{R}_b), \tag{1}$$

$$\frac{\partial \hat{T}_a}{\partial \hat{t}} = \frac{a\tau_{\text{bl}}}{C_a}(\hat{T}_s + \hat{T}_{\text{Top}} - 2\hat{T}_a) - c_{Dn}U(\hat{T}_a - \hat{T}_s)f(\hat{R}_b), \tag{2}$$

$$\frac{\partial \hat{T}_s}{\partial \hat{t}} = -1 + \frac{a\tau_{\text{bl}}}{C_v}(\hat{T}_a - \hat{T}_s) + \frac{a\tau_{\text{bl}}}{C_v}\left(\frac{\varepsilon_s}{\varepsilon_a} - 1\right)(\hat{T}_{\text{ref}} - \hat{T}_s) + \frac{C_a}{C_v}c_{Dn}\hat{U}(\hat{T}_a - \hat{T}_s)f(\hat{R}_b) - \frac{\lambda_m}{\delta_m}\frac{\tau_{\text{bl}}}{C_v}(\hat{T}_s - \hat{T}_m). \tag{3}$$

Also, the wind speed and the temperatures in $f(R_b)$ are scaled

$$f(\hat{R}_b) = \left(1 - \frac{\hat{R}_b}{\hat{R}_c}\right)^2; \qquad 0 \le \frac{\hat{R}_b}{\hat{R}_c} \le 1$$

$$f(\hat{R}_b) = 0; \qquad \frac{\hat{R}_b}{\hat{R}_c} > 1 \tag{4}$$

with

$$\hat{R}_b = \frac{\hat{T}_a - \hat{T}_s}{\hat{U}^2} \quad \text{and} \quad \hat{R}_c = R_c \frac{T_{\text{ref}}}{g(h/2 - z_0)}\frac{U_k^2}{T_k}.$$

This set of equations, describing the atmosphere–land interactions, is used in the analytical stability analysis.

3. Stability analysis of the equilibrium solution and derivation of the intermittency parameter

a. The equilibrium solution and its mathematical stability

Equations (1)–(3) contain three unknown variables $\hat{U}$, $\hat{T}_a$, and $\hat{T}_s$. These nonlinear differential equations have no general explicit solution. It is, however, possible to analyze the equilibrium solution of this system by setting the time derivatives to zero. A set of three nonlinear algebraic equations remains, which can be solved. The equilibrium solution of the system $\hat{U}_{\text{eq}}$, $\hat{T}_{a,\text{eq}}$, and $\hat{T}_{s,\text{eq}}$, as a function of the external parameters, is given in appendix C.

The model runs in Part I revealed that, in an equilibrium situation, the system is able to respond in two ways.

1) The system reaches a stable solution (in a mathematical sense), in which the values of $\hat{U}$, $\hat{T}_a$, and $\hat{T}_s$ reach their equilibrium values $\hat{U}_{\text{eq}}$, $\hat{T}_{a,\text{eq}}$, and $\hat{T}_{s,\text{eq}}$, as calculated in appendix C.
2) The system reaches an unstable solution, where the values of $\hat{U}$, $\hat{T}_a$, and $\hat{T}_s$ oscillate around their equilibrium values $\hat{U}_{\text{eq}}$, $\hat{T}_{a,\text{eq}}$, and $\hat{T}_{s,\text{eq}}$.

In this section the stability of the equilibrium solution is investigated with the help of so-called bifurcation techniques. For those not familiar with this type of stability analysis we give a very short outline in appendix F based on the excellent introductionary book on bifurcations by Seydel (1988). For a more rigorous treatment on Hopf bifurcations we refer to Hopf (1942) and Marsden and McCracken (1976). Readers not interested in the mathematical details may proceed to the example of section 3c.

In our analysis, the point of departure is the equilibrium solution of the system. The (local) stability of the system is investigated by applying a Taylor series expansion to the equations near this equilibrium point. This leads to a linear system of equations describing the behavior of $\hat{U}$, $\hat{T}_a$, and $\hat{T}_s$ near the equilibrium point. Information about the stability of the solution is obtained by evaluating the eigenvalues of the system. Positive eigenvalues correspond to solutions that are unstable in time. In the same way negative eigenvalues correspond to stable behavior and imaginary eigenvalues to cyclic/periodic behavior near the equilibrium point. The values of the eigenvalues depend on the actual values of the external parameters. One could, for example, analyze the model behavior while varying a certain parameter λ (e.g., pressure gradient). When λ passes some critical value λ_{crit}, a positive eigenvalue may change sign and the stable equilibrium point may turn into an unstable point. This qualitative change of the equilibrium solution when passing λ_{crit} is called branching or *bifurcation.* The type of bifurcation that connects a stable equilibrium with a periodic motion is called a Hopf bifurcation. The linearized system evaluated at the Hopf bifurcation point has a pair of purely imaginary eigenvalues $\pm i\beta$, which denotes the beginning of a cycle.

Because cyclic behavior for certain parameter ranges was found, it is assumed that in our system a Hopf bifurcation (HB) occurs. In this case two imaginary eigenvalues must exist for a certain combination of external variables. Reversing this argument, by setting this constraint on the eigenvalues the combination of external parameters can be found for which a transition in model behavior will occur. From that point it is possible to define a dimensionless number (denoted by Π) consisting of all external parameters, which defines, and thus predicts, the equilibrium behavior of the model. In section 3c it will be shown that the assumption about the existence of a Hopf bifurcation is valid.

b. Application of the Hopf bifurcation technique: Derivation of the intermittency parameter

In this section the Hopf bifurcation technique is applied to the SBL system described by Eqs. (1)–(3). The resulting dimensionless number is given explicitly in appendix D. The derivation of this number consists of the following steps.

- The starting point is a system consisting of three coupled nonlinear ordinary differential equations containing three unknown variables: $\hat{U}$, $\hat{T}_a$, and $\hat{T}_s$.
- The equilibrium situation for the system ($\partial\hat{U}/\partial\hat{t} = \partial\hat{T}_a/\partial\hat{t} = \partial\hat{T}_s/\partial\hat{t} = 0$) is solved. This gives the equilibrium values of the variables $\hat{U}_{\text{eq}}$, $\hat{T}_{a,\text{eq}}$, and $\hat{T}_{s,\text{eq}}$, as a function of the external parameters (appendix C).
- The system is linearized by making a Taylor expansion around the equilibrium situation. To this end the Jacobian of the system is calculated. Element A_{ij} of the Jacobian is defined by

$$A_{ij} = \frac{\partial F_i(x_1, x_2, x_3)}{\partial x_j} \qquad i = 1, 2, 3 \qquad j = 1, 2, 3, \tag{5}$$

  where F_i is the right-hand side of the ith equation [either (1), (2), or (3)], and $x_1 = \hat{U}$, $x_2 = \hat{T}_a$, and $x_3 = \hat{T}_s$. For example, A_{12} is the element consisting of the right-hand side of the equation for $\partial\hat{U}/\partial\hat{t}$ differentiated with respect to $\hat{T}_a$.
- The Jacobian is evaluated at the equilibrium point, so the equilibrium values $\hat{U}_{\text{eq}}$, $\hat{T}_{a,\text{eq}}$, and $\hat{T}_{s,\text{eq}}$ are substituted in the elements A_{ij}.
- In order to calculate the eigenvalues μ of the linearized system the characteristic polynomial of the Jacobian is calculated,

$$-\mu^3 - f_1\mu^2 - f_2\mu - f_3 = 0, \tag{6}$$

  where f_1, f_2, f_3 are the coefficients of the characteristic polynomial, which in turn are functions of the Jacobian elements A_{ij}.

The numerical results revealed a transition between stable and oscillatory behavior for a certain combination of external parameters. This leads to a crucial step in our derivation: we *assume* that this transition is a Hopf bifurcation (the assumption is verified below). Then, since at the Hopf bifurcation point the system should have two imaginary eigenvalues $\mu = \pm i\beta$, the characteristic polynomial *must* have the following form:

$$\pm(\mu^2 + \beta^2)(\mu + \alpha) = 0, \tag{7}$$

or, rewritten,

$$\mp(-\mu^3 - \alpha\mu^2 - \beta^2\mu - \alpha\beta^2) = 0. \tag{8}$$

Equating (6) and (8) (thus, noting $f_1 = \alpha$, $f_2 = \beta^2$, and

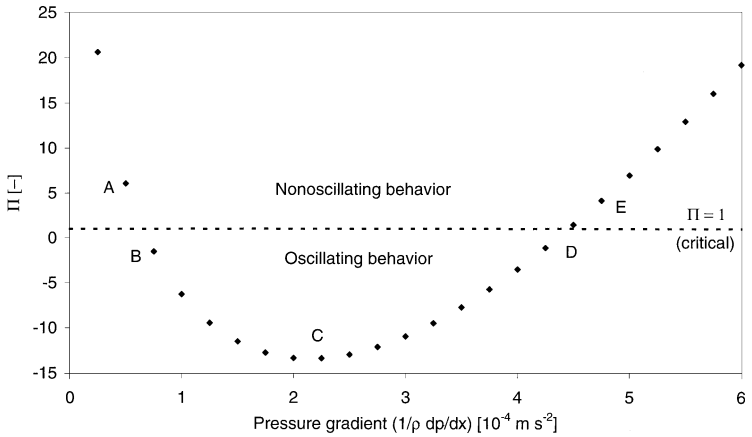

FIG. 2. The dimensionless intermittency parameter Π as a function of the pressure gradient. The critical level $\Pi = 1$, which separates two different types of system behavior, is given by the small dotted line.

$f_3 = \alpha\beta^2$) leads to a relation between the coefficients f_1, f_2, and f_3 at the HB point:

$$\frac{f_1 f_2}{f_3} = 1. \tag{9}$$

The left-hand side is a dimensionless group consisting of (all) external parameters that reaches a critical value of 1 at the HB point.

Formally, Eq. (9) is only valid *at* the HB point. Now, as a working hypothesis, we *extend* the findings of (9), by defining the left-hand side of (9) as a relevant dimensionless group characterizing the system behavior. Thus a classification parameter is proposed by (again, for the explicit form, see appendix D)

$$\Pi = \frac{f_1 f_2}{f_3}. \tag{10}$$

By definition $\Pi = 1$ at the HB point. Furthermore, it can be shown, by differentiating Π with respect to the eigenvalues, that, near the HB point, an unstable equilibrium corresponds to $\Pi < 1$ and a stable equilibrium to $\Pi \geq 1$. It is noted that the analysis above is done for the linearized system near the equilibrium. This means that, strictly speaking, no general statements can be made for the entire parameter space. However, from several thousands of runs, referring to a wide range a meteorological conditions, not a single example showed behavior that differed from the results of the local analysis presented above.

Thus, keeping in mind the restrictions of the analytical analysis, we generalize our results such that $\Pi < 1$ corresponds to periodic limit behavior and $\Pi \geq 1$ corresponds to stable limit behavior of the model.

c. An example

In this section the results of the analytical analysis above are compared with the results of the time-dependent solutions of the numerical model [i.e., Eqs. (B1)–(B3) of appendix B) to show that the predictions of the analytical analysis are supported by the numerical results. For details of these runs we refer to Part I. In Fig. 2 the value of the intermittency parameter Π is plotted as a function of the pressure gradient term. All other external parameters are kept constant (values given in Table 1 of Part 1). Our analytical analysis in the previous section showed that a transition in flow behavior is expected at $\Pi = 1$. In the case Fig. 2 refers to, Π equals 1 for two different values of $-1/\rho \times \partial P/\partial s$, notably at $-1/\rho \times \partial P/\partial s = 0.652 \times 10^{-4}$ and $-1/\rho \times \partial P/\partial s = 4.460 \times 10^{-4}$ (m s^{-2}). This means that if the pressure gradient is gradually increased from low to high values, two transitions in flow behavior are expected. To test this prediction, in Fig. 2 five points are selected in such a way that there is a point on each side of the flow transition. Besides these, an additional point in the middle of the pressure gradient axis is selected. The five points are denoted with the letters A–E, corresponding with runs A–E depicted in Figs. 3a and 3b. These runs are done with identical parameters (cf. Table 1 of Part I) except for the imposed pressure gradient, which is varied as in Fig. 2. It is noted that only equilibrium situations are considered, because the analytical solution is, strictly speaking (see discussion in Part I), only valid for the equilibrium situation. To assure equilibrium, results after 40 h of model time are shown.

A comparison of Figs. 3a and 3b with Fig. 2 shows that a transition in flow behavior appears to occur when Π crosses the critical value $\Pi = 1$, as predicted independently by the analytical model. Furthermore, the numerical runs show oscillating behavior in those cases where the dimensionless Π parameter is smaller than 1 and nonoscillating behavior for $\Pi \geq 1$. This is in agreement with the analytical predictions made by the local analysis near the Hopf bifurcation. The example in Fig. 2 is confined to runs where the pressure gradient was

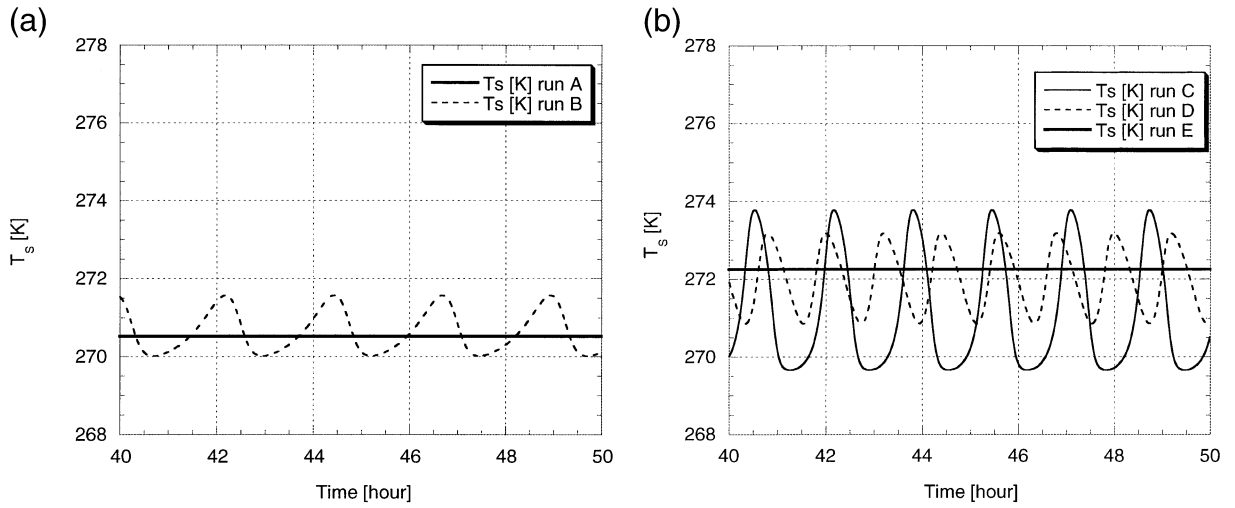

FIG. 3. (a) Equilibrium behavior of the surface temperature calculated by the numerical model, for two different values of the pressure gradient. Runs A and B correspond to cases A and B presented in Fig. 2. (b) Equilibrium behavior of the surface temperature calculated by the numerical model, for three different values of the pressure gradient. Runs C, D, and E correspond to cases C, D, and E presented in Fig. 2.

varied as an external parameter. Several thousands of additional runs were carried out for a wide range of external parameters. For all cases this again resulted in oscillating behavior for $\Pi < 1$ and nonoscillating behavior for $\Pi \geq 1$. Therefore strong evidence is found that, in the physically realistic parameter space, our local analysis of the nonlinear system can be generalized.

4. Flow regimes in the SBL: A classification based on dynamics

a. Classification based on SBL dynamics

We propose to use the dimensionless Π parameter as a classification parameter dividing equilibrium behavior into oscillatory behavior ($\Pi < 1$) and nonoscillatory behavior ($\Pi \geq 1$). Two important external parameters determining the equilibrium model behavior are the pressure gradient and the isothermal net radiation, because they control both the kinetic energy being supplied and the amount of negative buoyancy flux. Not only the equilibrium values of $\hat{U}$, $\hat{T}_a$, and $\hat{T}_s$, but also the stability of the equilibrium (in a mathematical sense) will be influenced by these parameters. As an illustration, the dependence of Π on the isothermal net radiation and the pressure gradient is given in a contour plot in Fig. 4. All points within the contour line of $\Pi = 1$ have values of Π lower than 1 and thus correspond to the oscillatory case. In the same way, points outside the line $\Pi = 1$ correspond to the nonoscillatory case. In Fig. 4 it is seen that in skies with little or no clouds, that is, situations with strong isothermal net radiation (-45 to -80 W m^{-2}), three regimes exist; compare section 3c. In fact, for such clear skies, the oscillating regime appears to split a single regime of nonperiodic flow (see Part I).

When in Fig. 4 the absolute value of the isothermal net radiation is decreased, a point is reached (about -45 W m^{-2}) where the oscillating regime does not exist whatever pressure gradient is imposed. In this situation the increased cloud cover reduces the loss of energy from the surface. This means that the instability mechanism sketched in the introduction (see also section 5) is less likely to occur and a nonoscillatory equilibrium situation will emerge. So in cases with moderate to large cloud cover only one regime with continuous turbulence exists. Note that this fact also agrees with the common observation that intermittent turbulence of the SBL occurs mostly during clear nights over land.

b. Relation to other SBL classifications

In the past a number of SBL classifications have been proposed. At present no general picture of SBL classification seems to exist. Most of the classifications reported in literature are based on static considerations rather than on dynamics. Some of these static indicators, based on similarity theory (such as z/L) proved to be very useful in classifying surface-layer measurements (Mahrt et al. 1998) and, more general, for classifying the SBL (Holtslag and Nieuwstadt 1986). Others propose static classification based on some form of a bulk Richardson number (e.g., Stull 1983; Revelle 1993).

The purpose of this section is to illustrate the fact that ''static'' indicators, such as the bulk Richardson number, provide different information about the equilibrium state than ''dynamic'' indicators, such as Π. But first we will show that a static indicator based on *external* parameters provides useful information about the same indicator calculated from *internal* variables. The

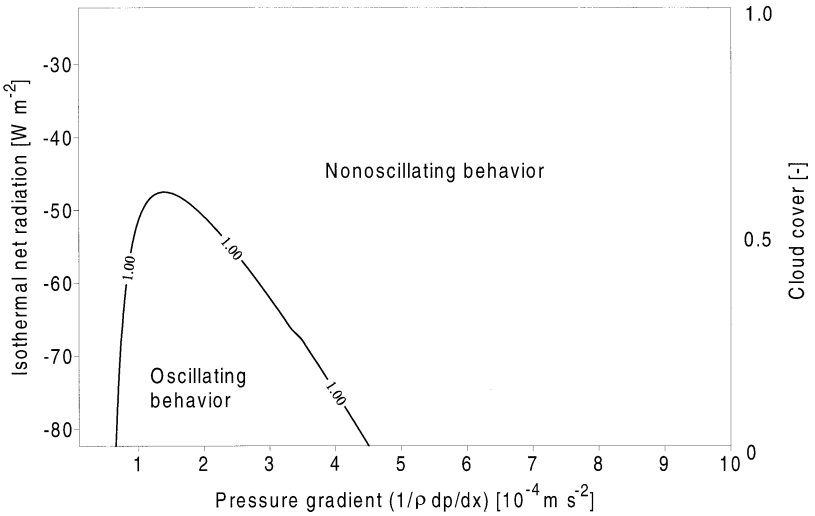

FIG. 4. Contour plot showing the dependence of the dimensionless intermittency parameter Π on the isothermal net radiation and on the pressure gradient. The critical level $\Pi = 1$ is given in a single contour line. For convenience, the cloud cover corresponding to the isothermal net radiation values is given on the right axis.

first static indicator for our system is defined as a so-called external bulk Richardson number,

$$R_{b,\text{ext}} = \frac{gz_{\text{sc}}}{T_{\text{ref}}} \frac{\Delta T_{\text{sc}}}{U_{\text{sc}}^2}, \tag{11}$$

where z_{sc}, ΔT_{sc}, and U_{sc} are the characteristic height scale, temperature scale, and velocity scale respectively.

- Recall that the boundary layer height h is taken as a typical height scale ($z_{\text{sc}} = h$).
- As a typical velocity scale we use $U_k/\sqrt{c_{Dn}}$. The division factor $\sqrt{c_{Dn}}$ is introduced to convert the velocity scale U_k (section 2) with a magnitude of order u_* to a velocity scale comparable with the logarithmic wind speed under neutral conditions.
- The temperature scale is defined as the temperature difference between T_a and T_s at radiative equilibrium of the soil surface. It can be derived from the longwave radiation budget by setting Q_{net} to zero and applying Taylor expansion around T_a. Thus a temperature scale ΔT_{sc} is found: $\Delta T_{\text{sc}} = (\varepsilon_s - \varepsilon_a^*)T_{\text{ref}}/4$ (see Holtslag and De Bruin 1988). Note that the temperature scale of section 2 (T_k) is not used, because of the fact that C_v is not a relevant parameter in the nonoscillating case.

Inserting the expressions for z_{sc}, ΔT_{sc}, and U_{sc} in (11) gives a simple estimate

$$R_{b,\text{ext}} = \frac{(\varepsilon_s - \varepsilon_a^*)}{-1/\rho \times \partial P/\partial s} \frac{gc_{Dn}}{4}; \qquad \varepsilon_a^* = \varepsilon_a + \frac{60N}{\sigma T_{\text{ref}}^4}, \tag{12}$$

where ε_a^* is the so-called apparent emissivity for the atmosphere. Next, $R_{b,\text{ext}}$ may be compared with the so-called internal bulk Richardson number $R_{b,\text{int}}$ calculated from the ''true'' equilibrium values of U, T_a, and T_s, under the same circumstances. The $R_{b,\text{int}}$ is defined as

$$R_{b,\text{int}} = \frac{gh}{T_{\text{ref}}} \frac{T_{a,\text{eq}} - T_{s,\text{eq}}}{U_{\text{eq}}^2}. \tag{13}$$

In Fig. 5 $R_{b,\text{int}}$ is plotted against $R_{b,\text{ext}}$. Figure 5 shows that there is a strong relationship between $R_{b,\text{int}}$ and $R_{b,\text{ext}}$, although at high values $R_{b,\text{ext}}$ becomes independent of $R_{b,\text{int}}$. This is the case because there is no limit on the value of $R_{b,\text{ext}}$, whereas $R_{b,\text{int}}$ has to stay below its critical value in order to keep a finite value of the surface friction to oppose the (small) pressure force.

In Fig. 5 different symbols are used for oscillatory and nonoscillatory equilibrium cases. It is observed that *both* oscillatory and nonoscillatory situations occur simultaneously for a broad range of $R_{b,\text{ext}}$ and $R_{b,\text{int}}$. This means that knowledge about a single bulk Richardson number only does not provide enough information about the (mathematical) stability of the system. Information about this stability can be gained by evaluation of Π (or, alternatively, by using additional information about another dimensionless number K, together with information about the bulk Richardson number; see section 5).

Nevertheless, it is noted that, roughly speaking, most oscillatory cases tend to occur in situations with high bulk Richardson numbers (Ri) and most nonoscillatory cases in situations with low bulk Richardson numbers. This result is in agreement with the observations of Kondo et al. (1978). They show that, with increasing Ri, a transition in flow behavior from nonintermittent to intermittent flow is expected. The transition between these flow regimes occurs for a rather broad range of Ri, as indicated in Fig. 5.

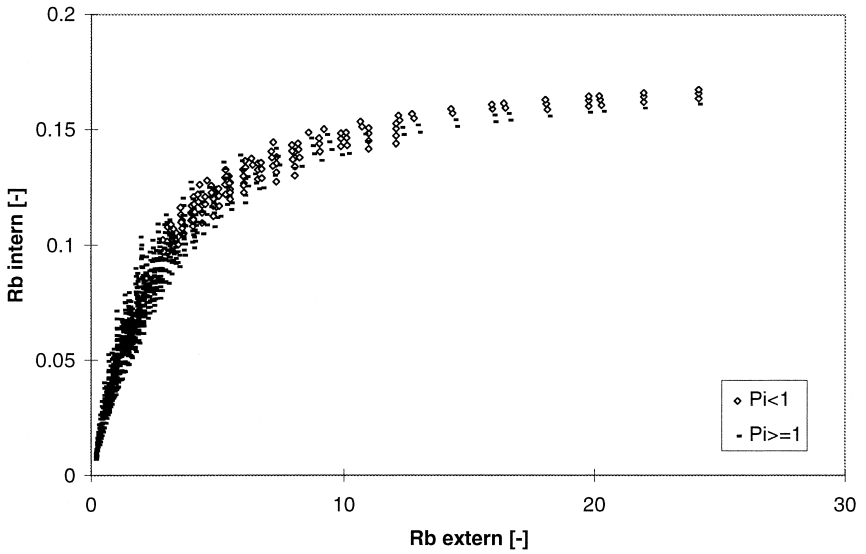

FIG. 5. Internal bulk Richardson number, calculated from the equilibrium values of U, T_a, and T_s, plotted against the external bulk Richardson number, calculated from external parameters. Oscillatory cases ($\Pi < 1$) and nonoscillatory cases ($\Pi \geq 1$) are denoted with different symbols.

5. A simplified criterion for instability

a. Introduction

In section 3 the instability criterion (i.e., $\Pi = 1$) for the SBL system given by Eqs. (1)–(3) was derived formally. Although application of this formal criterion gives an exact prediction of the actual stability of the system, it does not provide insight into the physical background of the instability mechanism, due to the complex form of Π. Therefore, in this section, a less exact but simpler stability criterion is given, which does allow a physical interpretation.

The simplified criterion for instability is derived by application of a fixed shear criterion for instability (FSCI; Derbyshire 1999). To this end the unscaled temperature equations for T_a and T_s of appendix B are combined into a single equation, describing the time evolution of the temperature gradient $(T_a - T_s)$. We consider near-equilibrium situations with no net flux to the combined atmosphere–surface system. As such $a(T_{\text{Top}} - T_a) = -(Q_i + G)$ and we assume T_{ref} to be close to T_s. In that case the combined equation reads

$$\frac{d(T_a - T_s)}{dt} = m\left\{-\left[Q_i - \frac{\lambda_m}{\delta_m}(T_s - T_M)\right] - a(T_a - T_s) - \rho c_p c_{Dn}(T_a - T_s)Uf(R_b)\right\}, \qquad (14)$$

with $m = 1/C_v + 1/C_a$.

Equation (14), together with the momentum equation [Eq. (B1), appendix B] forms our new simplified system. As an approximation, the stability of this system is investigated by studying the response of Eq. (14) to an initial disturbance in $(T_a - T_s)$, keeping U fixed at its equilibrium value (FSCI). In this way, we find that the system is unstable when

$$\left\{\frac{\partial}{\partial(T_a - T_s)}\left[\frac{d(T_a - T_s)}{dt}\right]\right\}_{\text{eq}} > 0. \qquad (15)$$

Thus, the rhs of (14) is differentiated to $(T_a - T_s)$: a positive value refers to a positive feedback, namely, that any disturbance in $(T_a - T_s)$ is enhanced, leading to instability. Obviously, in the same manner, a negative value indicates a negative feedback stabilizing the system.

A physical interpretation of (15) is possible in terms of the surface energy balance, represented by the rhs of (14). For example, a sudden cooling of the surface (by a small disturbance from the equilibrium), results in an increase of the stratification $(T_a - T_s)$. The decrease in T_s causes a compensating temporal increase in the soil heat flux, in the radiative heat flux [outside the atmospheric window, i.e., $a(T_a - T_s)$], and in the downward turbulent heat flux. These compensating fluxes counteract the sudden cooling, forming a negative feedback, which stabilizes the system (mathematically speaking).

In conditions of strong stratification (high Ri), however, the turbulent heat flux may *decrease* in spite of an increasing temperature gradient, due to the limiting effect of stratification on mixing efficiency (see also De Bruin 1994; Malhi 1995). If this effect is large compared to the compensating effects by the soil heat flux and the radiative heat flux, this will cause an increase in the energy loss at the surface. This leads to an *amplification* of the disturbance in $(T_a - T_s)$ from the equilibrium, causing instability.

Before we derive the fixed shear criterion for insta-

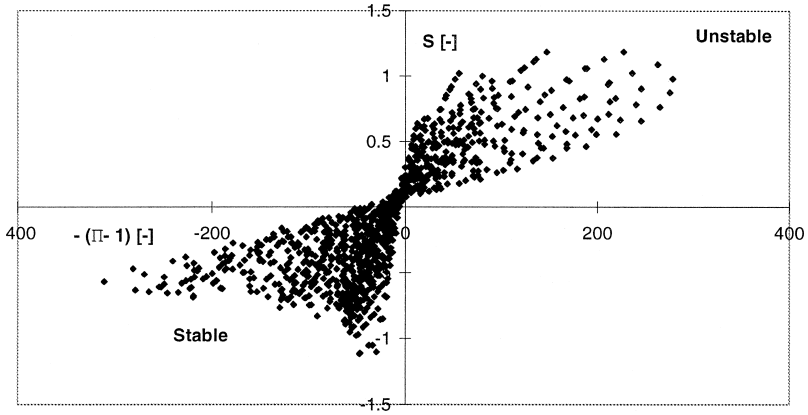

FIG. 6. Comparison of the approximated stability criterion S vs the exact stability criterion $-(\Pi - 1)$.

bility it is noted that we confine ourselves to cases with $C_v \ll C_a$, also assuming a small heat capacity of the vegetation compared to the thick soil layer, so that the amplitude in T_s is large compared to the amplitudes in T_a and T_M (see Part I). This means that $d(T_s - T_M) \approx -d(T_a - T_s)$. Now, criterion (15) is applied to (14), keeping the wind speed at its equilibrium value. The equilibrium wind speed can be found from Eq. (B1) of appendix B so that the results can be expressed in terms of R_b. Thus it is found that the system is unstable (oscillating) if

$$\left\{\frac{R_b}{R_c}\right\}_{\text{eq}} > \frac{(K + 1)}{3}, \tag{16}$$

with

$$K = \frac{a + \lambda_m/\delta_m}{\rho c_p \sqrt{c_{Dn}} \times \sqrt{P_g h}} \quad \text{and}$$

$$P_g = -\frac{1}{\rho}\frac{\partial P}{\partial s} \quad \text{(for brevity)}.$$

It is observed that the criterion for instability (16) depends on *two dimensionless groups*:

1) the normalized equilibrium bulk Richardson number $(R_b/R_c)_{\text{eq}}$, and
2) the partitioning parameter K.

Both groups can easily be calculated from the external variables. In appendix E the expression of the first group $(R_b/R_c)_{\text{eq}}$ is given in terms of the radiative forcings and of the (ageostrophic) pressure gradient.

The second dimensionless group K, which we will denote as the ''partitioning parameter,'' is physically interpreted as the ratio of the summed radiative and soil heat exchange coefficient compared to the exchange coefficient for turbulent heat transport (or, alternatively, the ratio of fluxes). As mentioned before, a large exchange coefficient for longwave radiation and for soil heat flux counteracts the effect of a decreasing exchange coefficient of the turbulent heat flux at high Ri. Contrary to the turbulent heat flux, radiative and soil heat flux increase monotonically with an increasing temperature gradient. Thus, as in many physical problems (e.g., cf. the Rayleigh number), a large ''diffusive'' component prevents physical instability.

Note from (16) that application of the FSCI to turbulent heat flux *only* would result in $R_b/R_c \geq 1/3$ as a criterion for instability. However, taking the effects of soil heat flux and radiative heat flux into account, we observe that $R_b/R_c \geq 1/3$ is merely a necessary condition for instability, not a sufficient condition. This confirms the findings of section 4b, namely, that instability is more likely to occur at high Richardson numbers but also that the bulk Richardson number is not the only parameter determining the dynamic behavior (stability) of the system.

b. Comparison of stability criteria

In this section the simplified stability criterion given by Eq. (16) is compared with the detailed Π criterion. To this end we define a parameter S as

$$S = \{R_b/R_c\}_{\text{eq}} - (K + 1)/3.$$

Thus, positive values of S indicate instability. In Fig. 6 the value of S is plotted against $-(\Pi - 1)$, for a large number of different parameter sets. The transformation $-(\Pi - 1)$ is chosen instead of Π, to assure that negative values of $-(\Pi - 1)$ correspond to stable cases and positive values with unstable cases, as is the case with S. If there were an exact agreement between both stability indicators, the ''butterfly'' of Fig. 6 should exactly be located in the first and the third quadrant, with a crossing through the origin. Thus, it is observed that the agreement between the two stability criteria is rather good. Only for the points near the origin (i.e., the weakly intermittent cases with small amplitudes) a slight disagreement between the criteria is present due to the approximations in the derivation of S [especially the

assumption of a fixed shear, whereas in reality disturbances in stratification strength affect U_{eq}; see also Derbyshire (1999)]. Thus, it is concluded that the simplified criterion given by (16) is good approximation for the detailed Π criterion.

6. Discussion

a. Intermittency vs decoupling

The present study has some parallels with the recent study of Derbyshire (1999), who studied the so-called decoupling phenomenon of the SBL over cold surfaces. He defines the decoupling as a cessation of turbulent transport between the surface and the atmosphere due to high stability. Decoupling of the SBL is strongly related to intermittent SBL behavior, with the exception that in the latter case the SBL recovers after decoupling due to an acceleration of the air by the pressure gradient, ultimately causing a turbulence burst. Actually, an example shown by Derbyshire (1999, his Fig. 9) shows a recovery from a very small heat flux twice. Generally, the present study agrees with the results of Derbyshire. Both studies reveal a strong sensitivity of the (dynamic) stability of the SBL to the radiative forcing, the pressure gradient, the thermal properties of the (vegetated) surface, and its roughness (see Part I). Also the importance of the shape of the stability functions [$f(R_b)$] on the dynamic stability is recognized in both studies.

Derbyshire (1999) addresses the possibility of a positive feedback in the cooling of the surface: in the presence of a strong stratification, an increase in stratification causes a decrease in turbulent heat exchange so that the surface cooling is enhanced even further. In both the present study and in the study of Derbyshire the possibility of this feedback phenomenon is studied in approximation by investigation of a so-called fixed shear criterion for instability (FSCI). The main difference between the FSCI in both studies lies in the fact that Derbyshire (1999) concentrates on the instability criterion in terms of the *turbulent heat flux*, whereas in the present study the FSCI is interpreted in terms of the so-called *energy supply*, which, in addition to the turbulent heat flux, includes the effect of the radiative and soil heat exchange.

With the help of this energy supply concept, the SBL classification of Fig. 6 is interpreted as follows: for every possible combination of the pressure gradient and the isothermal net radiation an equilibrium solution can be found (ranging from a ''near-neutral'' equilibrium with high turbulent fluxes to a radiative equilibrium with no turbulent fluxes). However, for a fixed value of the pressure gradient, there is a certain maximum value of the isothermal radiation that can be supplied by a stationary energy supply. In case a higher value of the isothermal radiation is imposed on the system, the system will compensate this with an oscillatory energy supply, reflected by intermittent turbulence.

b. Impact of the boundary conditions

McNider et al. (1995) used a simplified, two-layer SBL model, with the same kind of parameterization as presented in this text, to study SBL dynamics. In order to study SBL dynamics, they used numerical bifurcation techniques (unlike our analytical approach). They report some oscillatory behavior of the mean variables for certain parameter ranges, which confirms the results of this study. Contrary to our results, however, they report double-valued equilibrium solutions for certain values of the external parameters. For example, two values of U_{eq}, $T_{a,eq}$, and $T_{s,eq}$ and found for a particular combination of external parameters. The existence of multiple solutions could have strong implications for the predictability of the SBL in the sense that even slight changes in initial conditions would lead to quite different solutions for temperature and wind speed.

The difference in model behavior between both studies can be explained by the use of different boundary conditions. In our study at the upper model boundary the turbulent fluxes are assumed to be zero (prescribed fluxes). In the study of McNider et al. at the model boundary the potential temperature and the wind speed (geostropic) are prescribed, allowing turbulent interaction between the actual model and the higher levels. Imposing this kind of boundary condition, basically two type of equilibrium solutions are possible. 1) The overlying air is decoupled from the model layer. In this case the equilibrium solution of the model basically follows our results, where the momentum of the model layer is supplied by the pressure force. 2) The overlying air interacts with the model layer. In this situation extra momentum and heat from above are supplied to the model domain, resulting in an equilibrium solution different from the situation without this transport.

The comparison between the present study and the study of McNider et al. shows that a possible interaction between the upper air and the near-surface air allows a larger number of dynamical cases than the specific cases discussed in this paper. Therefore, from both a modeling and observational point of view (see below), there is a need for studying the possibility of an interaction between the high-level shear and the ASI, as presented here.

c. Practical issues

The classification proposed in the previous sections can be used as a framework to study observations of different SBL regimes. In the previous section we already emphasized that the present analysis is valid for a special class of SBLs. We assumed fluxes to decrease with height and assumed no interaction of the near-surface layer with elevated shear layers. Also, due to the idealized structure of the bulk model, a comparison with observational data is not straightforward. Below a few examples are given.

1) The boundary layer height is a prescribed (external) variable, whereas in reality this height is a dependent (internal) system variable.
2) Coriolis effects are neglected, which means that the imposed pressure gradient in fact represents an effective pressure gradient in the (nonfixed) direction of the mean wind speed.
3) The analytical derivation of Π is, strictly speaking, only valid for an equilibrium situation. In reality, however, the nocturnal boundary layer keeps on cooling all night, so that a real equilibrium is not reached (e.g., Nieuwstadt and Tennekes 1981). Nevertheless, the results may be extended to quasi-steady situations (see Part I).
4) Bulk approaches are used to calculate fluxes. This means that model results have to be compared with measured bulk variables, rather than with local profiles. This will smooth out a lot of detail.

It is challenging to release some of these (strict) assumptions in future theoretical work. At the same time, it is challenging to investigate the relation between the ASI and other mechanisms that can generate oscillations and intermittent turbulence, such as gravity waves and shear flow instabilities near the level of the wind maximum.

7. Conclusions

In the stable boundary layer, discontinuous, intermittent turbulence can be generated by a direct atmosphere–surface interaction without interaction with the air aloft. This intermittency mechanism is associated with the most essential elements of the SBL: the build up of stratification by strong surface cooling, the supply of mechanical energy by the synoptic pressure gradient, and the limiting effect of stratification on mixing efficiency. In a companion paper (Part I), model simulations show that the essence of this intermittent behavior can be captured by simplifying the SBL to a system of three coupled nonlinear differential equations describing the time evolution of wind speed, air temperature, and surface temperature. In the present study the same system is studied analytically in order to get more insight into the physical mechanism of this intermittent SBL behavior. The analysis resulted in the conclusions mentioned below.

The system dynamic analysis shows that, from a mathematical point of view, the transition from a continuous turbulent regime to a discontinuous, intermittent regime can be explained as a Hopf bifurcation connecting a nonoscillatory and an oscillatory state of the system. This property is used in the derivation of a dimensionless intermittency parameter (Π), from which the equilibrium behavior of the system (i.e., oscillatory or nonoscillatory) can be predicted exactly. As for the equilibrium solution, the intermittency parameter can be directly evaluated from the values of the external parameters. As such, this parameter is used to classify SBL behavior. It is also shown that this classification, based on dynamic SBL behavior, differs from classifications based on static stability parameters such as z/L or on a single Richardson number.

In the present study, a physical explanation for the instability mechanism that leads to intermittent SBL behavior was given in terms of a fixed shear criterion for instability (FSCI; Derbyshire 1999). The analysis shows that in most cases SBL instability is caused by the following positive feedback. In cases where a strong stratification is present, the magnitude of the turbulent heat flux *decreases* with increasing stratification, due to the fact that under strong stratification the limiting effect of stratification on turbulent heat transport becomes more important than the increase in temperature gradient. This means that a positive disturbance on the stratification causes a smaller heat flux, which means that less energy is supplied to the surface, enhancing the stratification and thus enhancing the disturbance.

In addition, it was shown that high values of the exchange coefficient for radiative transport and for the soil/vegetation heat flux have a stabilizing effect on the system because they prevent a rapid change of the surface temperature. This confirms the results of Part I, showing the importance of vegetation thermal characteristics on the intermittency dynamics.

For the system described in Part I an explicit equilibrium solution is found. The solution gives the equilibrium values of the internal parameters (wind speed, air temperature, and surface temperature) and of the fluxes (turbulent heat flux, net radiation, and soil heat flux) as a function of the external forcing parameters. Therefore, this equilibrium solution may provide a useful starting point for future flux parameterizations in terms of external parameters.

A critical remark is made regarding the generality of the present results. Although the intermittency mechanism arising from a positive feedback between stratification and mixing efficiency in shear flow is an important candidate explaining the observed intermittency in SBLs, it is presently not clear whether this intermittency is caused by a direct surface–atmosphere interaction (present work), if the intermittency is formed in shear layers higher up (Vukelic and Cuxart 2000; Ha and Mahrt 2001), or by a combination of both. The present work only provides a framework for the first case. It would be challenging to extend the present framework to the more general case, allowing both atmosphere–surface interaction and interaction with higher shear layers.

Finally, there is a strong need for experimental research on the occurrence of intermittency in stable boundary layers. Extensive measurement campaigns such as CASES99 (Poulos et al. 2000) may help to improve our knowledge about the generation of these intermittent events. Also, the observations might answer the question of how the intermittency mechanism de-

cribed in this work is related to other intermittency generating mechanisms such as wave-induced turbulence and high-level shear instabilities. Finally, in order to understand under what circumstances an intermittent character of turbulence near the surface is to be expected, a classification based on observations of different SBL regimes under different synoptic conditions would be of great value.

Acknowledgments. The authors wish to thank Richard McNider, Onno van Herwaarden and Peter Duynkerke for reading the manuscript and/or providing useful suggestions.

APPENDIX A

Symbol List

Apart from the conventional notation (e.g., for g, z_0, ε_a, κ, σ, see Part I) the following symbols are used.

α	Real eigenvalue of Jacobian (−)
a	Longwave radiation exchange coefficient (−)
A_{ij}	Element of the Jacobian (−)
β	Imaginary eigenvalue of Jacobian (−)
c_{Dn}	Neutral drag coefficient (−)
C_a	Heat capacity of the air column per unit area (J m^{-2} K^{-1})
C_v	Heat capacity of the vegetation layer per unit area (J m^{-2} K^{-1})
δ_m	Thickness of the thin mulch layer (m)
d	Height of the vegetation layer (m)
G_0	Soil heat flux (W m^{-2})
h	Depth of the turbulent boundary layer (m)
H	Sensible heat flux (W m^{-2})
K	Partitioning parameter (−)
λ	Bifurcation parameter (units)
λ_m	Conductivity of the thin mulch layer (W K^{-1} m^{-1})
m	Inverse weighted heat capacity (K m^2 J^{-1})
μ	Dummy element of characteristic polynomial (−)
N	Fraction of cloud cover (−)
Π	Intermittency parameter (−)
P_g	(Acceleration due to) pressure gradient (m s^{-2})
Q_i	Isothermal (or maximum) net radiation (W m^{-2})
Q_{net}	Net radiation (W m^{-2})
R	Longwave radiative component (W m^{-2})
R_b	Bulk Richardson number (−)
$\hat{R}_b$	Scaled bulk Richardson number (−)
R_c	Critical bulk Richardson number (−)
$\hat{R}_c$	Modified critical bulk Richardson number (−)
s	Distance (m)
S	Simplified stability parameter (FSCI) (−)
τ	Shear stress (N m^{-2})
τ_{bl}	Boundary layer timescale (s)
$\hat{t}$	Scaled time (−)
T_a	(Height averaged) air temperature (K)
$\hat{T}_a$	Scaled air temperature (−)
T_k	Temperature scale (K)
T_{ref}	Reference temperature (K)
T_s	Surface temperature (K)
$\hat{T}_s$	Scaled surface temperature (−)
T_{Top}	Temperature of atmosphere above the turbulent boundary layer (K)
U	(Height averaged) wind speed (m s^{-1})
$\hat{U}$	Scaled wind speed (−)
U_k	Velocity scale (m s^{-1})

APPENDIX B

The Unscaled System Equations

Our simplified system derived in Part I is based on three coupled nonlinear differential equations for U, T_a, and T_s. They read as

$$\frac{\partial U}{\partial t} = -\frac{1}{\rho}\frac{\partial P}{\partial s} - \frac{1}{h}\frac{\kappa^2}{\left[\ln\left(\frac{h/2}{z_0}\right)\right]^2}U^2 f(R_b), \tag{B1}$$

$$\frac{\partial T_a}{\partial t} = \frac{4\varepsilon_a \sigma T_{\text{ref}}^3 (T_s + T_{\text{Top}} - 2T_a)}{C_a} - \frac{\rho c_p}{C_a}\frac{\kappa^2}{\left[\ln\left(\frac{h/2}{z_0}\right)\right]^2}U(T_a - T_s) f(R_b), \tag{B2}$$

$$\frac{\partial T_s}{\partial t} = \frac{-\sigma(\varepsilon_s - \varepsilon_a)T_{\text{ref}}^4 + 60N}{C_v} + \frac{4\varepsilon_a \sigma T_{\text{ref}}^3}{C_v}(T_a - T_s) + \frac{4\varepsilon_a \sigma T_{\text{ref}}^3}{C_v}\left(\frac{\varepsilon_s}{\varepsilon_a} - 1\right)(T_{\text{ref}} - T_s) + \frac{\rho c_p}{C_v}\frac{\kappa^2}{\left[\ln\left(\frac{h/2}{z_0}\right)\right]^2}U(T_a - T_s) f(R_b) - \frac{1}{C_v}\frac{\lambda_m}{\delta_m}(T_s - T_M), \tag{B3}$$

with

$$f(R_b) = \left(1 - \frac{R_b}{R_c}\right)^2 = \left(1 - \frac{1}{R_c}\frac{g[(h/2) - z_0]}{T_{\text{ref}}}\frac{T_a - T_s}{U^2}\right)^2; \qquad 0 \le \frac{R_b}{R_c} \le 1$$

$$f(R_b) = 0; \qquad \frac{R_b}{R_c} > 1. \tag{B4}$$

APPENDIX C

The Equilibrium Solution

The equilibrium solution of the system [Eqs. (B1)–(B3), appendix B] is given below. Note that the equi-

librium values of all the fluxes (e.g., H_{eq}, $u_{*,eq}$) can be calculated directly from $\hat{U}_{eq}$, $\hat{T}_{a,eq}$, and $\hat{T}_{s,eq}$:

$$\hat{U}_{eq} = -\frac{b}{2} + \frac{1}{2}\sqrt{b^2 - 4c},$$

$$\hat{T}_{a,eq} = -(\hat{U} - \delta)\left(\frac{C_a\hat{R}_c}{a\tau_{bl}}\right)\frac{\alpha}{1 + 2\alpha} + \gamma,$$

$$\hat{T}_{s,eq} = (\hat{U} - \delta)\left(\frac{C_a\hat{R}_c}{a\tau_{bl}}\right)\frac{1}{1 + 2\alpha},$$

in which

$$b = \left(\frac{C_a}{a\tau_{bl}}\right)\frac{\alpha + 1}{2\alpha + 1} - \sqrt{c_{Dn}}$$

$$c = -\delta\left(\frac{C_a}{a\tau_{bl}}\right)\frac{\alpha + 1}{2\alpha + 1} - \frac{\gamma}{\hat{R}_c},$$

$$\alpha = \left(\frac{\varepsilon_s}{\varepsilon_a} - 1\right) + \left(\frac{\lambda_m/\delta_m}{a}\right)$$

$$\delta = \left(\frac{a\tau_{bl}}{C_a}\right)\frac{1}{\hat{R}_c}(T_{Top} - 2\gamma) + \sqrt{c_{Dn}},$$

$$\gamma = -1\left(\frac{C_v}{a\tau_{bl}}\right) + \hat{T}_{Top} + \hat{T}_{ref}\left(\frac{\varepsilon_s}{\varepsilon_a} - 1\right) + \hat{T}_M\left(\frac{\lambda_m/\delta_m}{a}\right).$$

APPENDIX D

Explicit Form Pi Parameter

Following the derivation of section 3, Π is given by

$$\Pi = \frac{f_1 f_2}{f_3},$$

with

$$f_1 = -A_{11} - A_{22} - A_{33},$$

$$f_2 = A_{11}A_{22} + A_{22}A_{33} + A_{11}A_{33} - A_{32}A_{23} - A_{31}A_{13} - A_{21}A_{12},$$

$$f_3 = -A_{11}A_{22}A_{33} + A_{32}A_{23}A_{11} + A_{21}A_{12}A_{33} - A_{21}A_{32}A_{13} - A_{31}A_{12}A_{23} + A_{31}A_{22}A_{13}.$$

Next the matrix elements of the Jacobian are given. In order to keep the matrix elements compact, Eq. (B1) is substituted when possible:

$$A_{11} = -\frac{2}{\hat{U}} - 4\frac{\sqrt{c_{Dn}}}{\hat{R}_c}\frac{\hat{T}_a - \hat{T}_s}{\hat{U}^2}$$

$$A_{21} = -\frac{\hat{T}_a - \hat{T}_s}{\hat{U}^2} - 4\frac{\sqrt{c_{Dn}}}{\hat{R}_c}\frac{(\hat{T}_a - \hat{T}_s)^2}{\hat{U}^3}$$

$$A_{12} = 2\frac{\sqrt{c_{Dn}}}{\hat{R}_c}\frac{1}{\hat{U}}$$

$$A_{22} = -2\frac{a\tau_{bl}}{C_a} - \frac{1}{\hat{U}} + 2\frac{\sqrt{c_{Dn}}}{\hat{R}_c}\frac{\hat{T}_a - \hat{T}_s}{\hat{U}^2}$$

$$A_{13} = -2\frac{\sqrt{c_{Dn}}}{\hat{R}_c}\frac{1}{\hat{U}}$$

$$A_{23} = \frac{a\tau_{bl}}{C_a} + \frac{1}{\hat{U}} - 2\frac{\sqrt{c_{Dn}}}{\hat{R}_c}\frac{\hat{T}_a - \hat{T}_s}{\hat{U}^2}$$

$$A_{31} = \frac{C_a}{C_v}\frac{\hat{T}_a - \hat{T}_s}{\hat{U}^2} + 4\frac{C_a}{C_v}\frac{\sqrt{c_{Dn}}}{\hat{R}_c}\frac{(\hat{T}_a - \hat{T}_s)^2}{\hat{U}^3}$$

$$A_{32} = \frac{a\tau_{bl}}{C_v} + \frac{C_a}{C_v}\frac{1}{\hat{U}} - 2\frac{C_a}{C_v}\frac{\sqrt{c_{Dn}}}{\hat{R}_c}\frac{\hat{T}_a - \hat{T}_s}{\hat{U}^2}$$

$$A_{33} = -\frac{a\tau_{bl}}{C_v} - \frac{a\tau_{bl}}{C_v}\left(\frac{\varepsilon_s}{\varepsilon_a} - 1\right) - \frac{C_a}{C_v}\frac{1}{\hat{U}} + 2\frac{C_a}{C_v}\frac{\sqrt{c_{Dn}}}{\hat{R}_c}\frac{\hat{T}_a - \hat{T}_s}{\hat{U}^2} - \frac{\lambda_m}{\delta_m}\frac{\tau_{bl}}{C_v}.$$

The values of $\hat{U}$, $\hat{T}_a$, and $\hat{T}_s$ at the equilibrium point are given by $\hat{U}_{eq}$, $\hat{T}_{a,eq}$, and $\hat{T}_{s,eq}$ as presented in appendix C.

APPENDIX E

The Equilibrium Bulk Richardson Number

In order to evaluate the stability criterion of section 5 an expression for the normalized bulk Richardson number is needed. The equilibrium value of R_b/R_c as a function of ''external'' variables can be derived from Eq. (14) in combination with the unscaled momentum equation [Eq. (B1)]:

$$\left(\frac{R_b}{R_c}\right)_{eq} = 1 + \frac{(\sigma^* - 1) - \sqrt{(\sigma^* - 1)^2 + 4\sigma^*(\delta^* + 1)}}{2(\delta^* + 1)},$$

with

$$\delta^* = \frac{-(Q_i + G)}{\rho c_p}\frac{1}{P_g h}\frac{\sqrt{c_{Dn}}}{\sqrt{P_g h}}\frac{1}{R_c} \quad \text{and}$$

$$\sigma^* = \frac{a}{\rho c_p\sqrt{c_{Dn}}\sqrt{P_g h}}.$$

Here δ^* can be interpreted as the maximum normalized bulk Richardson number, determined by the available amount of energy ($Q_i + G$). This amount is divided into 1) turbulent heat flux and 2) radiative heat flux (outside the window region). Further, σ^* can be interpreted as the ratio between the exchange coefficient for radiation and the exchange coefficient for turbulent heat flux.

It is noted that G is not a real external parameter, in a sense that it can be determined beforehand. However, additional analysis showed that in our model system it could easily be parameterized in terms of Q_i by $G = \alpha Q_i$, with $\alpha = (\lambda_m/\delta_m)/((\lambda_m/\delta_m) + a)$.

APPENDIX F

Outline of the Hopf Bifurcation Technique

Because the Hopf bifurcation technique is not commonly used in atmospheric sciences, and because of the fact that it forms the core of the work presented in this article, it will be explained rather basically. The condensed explanation is based on the introductary book of Seydel (1988).

As an example a system with two coupled nonlinear ordinary differential equations is considered:

$$\frac{dy_1}{dt} = f_1(y_1, y_2), \qquad \frac{dy_2}{dt} = f_2(y_1, y_2). \tag{F1}$$

Equilibrium points of this system are reached when the time derivatives are zero. The system presented above is solved for this condition, which gives the values of the equilibrium points y_1^{eq} and y_2^{eq}. One could get (local) information about the behavior of the system near the equilibrium by disturbing the equilibrium values. Now it is the differential equations that decide whether the trajectories, or $y_1(t)$ and $y_2(t)$, starting in the vicinity of y_1^{eq} and y_2^{eq}, remain near the equilibrium (attraction) or depart from it. To start a local analysis of the behavior of the equations a Taylor series expansion of f_1 around (y_1^{eq}, y_2^{eq}) gives

$$\begin{aligned}\frac{dy_1}{dt} &= f_1(y_1, y_2)\\ &= f_1(y_1^{eq}, y_2^{eq}) + \frac{\partial f_1(y_1^{eq}, y_2^{eq})}{\partial y_1}(y_1 - y_1^{eq})\\ &\quad + \frac{\partial f_2(y_1^{eq}, y_2^{eq})}{\partial y_2}(y_2 - y_2^{eq}) + \text{h.o.t.}\end{aligned} \tag{F2}$$

Expanding also the f_2 of the second differential equation, observing that $f_1(y_1^{eq}, y_2^{eq}) = f_2(y_1^{eq}, y_2^{eq}) = 0$, and dropping the higher-order terms gives two differential equations that are *linear* in $(y_1 - y_1^{eq})$ and $(y_2 - y_2^{eq})$. Because the equations are linear, they can easily be solved with the help of standard theory as we will show. The linearized system is easily written down in matrix notation if one uses the derivative or *Jacobian* matrix:

$$\mathbf{J} = \begin{Bmatrix} \dfrac{\partial f_1(y_1^{eq}, y_2^{eq})}{\partial y_1} & \dfrac{\partial f_1(y_1^{eq}, y_2^{eq})}{\partial y_2} \\ \dfrac{\partial f_2(y_1^{eq}, y_2^{eq})}{\partial y_1} & \dfrac{\partial f_2(y_1^{eq}, y_2^{eq})}{\partial y_2} \end{Bmatrix}. \tag{F3}$$

If the vector $\mathbf{h}$ is represented by

$$h_1(t) \approx y_1(t) - y_1^{eq}(t) \qquad h_2(t) \approx y_2(t) - y_2^{eq}(t), \tag{F4}$$

then the above-mentioned linearized system can be written as

$$\frac{d\mathbf{h}}{dt} = \mathbf{J} \cdot \mathbf{h}. \tag{F5}$$

So this equation describes how the system evolves when the initial state deviates slightly from its equilibrium values. As in standard theory about systems of linear ordinary differential equations, one tries to solve the system by stating the following hypothesis about the form of its solution:

$$\mathbf{h}(t) = \begin{bmatrix} h_1(t) \\ h_2(t) \end{bmatrix} = \begin{bmatrix} C_{11} \\ C_{12} \end{bmatrix} e^{\mu_1 t} + \begin{bmatrix} C_{21} \\ C_{22} \end{bmatrix} e^{\mu_2 t}. \tag{F6}$$

By inserting this solution in (F5) it can be shown that this problem is equivalent to a eigenvalue problem. The two eigenvalues μ_1 and μ_2 that meet the above stated hypothesis are the solutions of the characteristic equation

$$\det(\mathbf{J} - \mu \cdot \mathbf{I}) = 0. \tag{F7}$$

Now several situations can occur.

- The μ_1 and μ_2 are positive. Then the argument of the exponents in Eq. (F6) are positive, any disturbance grows with time, which will give rise to an *unstable* equilibrium.
- There μ_1 and μ_2 are both negative. In a similar way this leads a *stable* equilibrium.
- Either μ_1 or μ_2 is negative and the other positive. The equilibrium point will be a so-called saddle point.
- The μ_1 and μ_2 are both complex. Then any trajectory close to the equilibrium resembles a spiral.

Parameter dependence

Usually a differential equation describing a real meteorological problem involves one or more parameters. Denoting one such parameter by λ, the differential equations read

$$\frac{dy_1}{dt} = f_1(y_1, y_2, \lambda) \qquad \frac{dy_2}{dt} = f_2(y_1, y_2, \lambda). \tag{F8}$$

Because this system depends on the actual value of λ we speak of a family of differential equations. So solutions $\mathbf{y}(t; \lambda)$ of the system now depend both on t and λ.

Consequently, equilibrium points, Jacobian matrices, and the eigenvalues μ depend on λ:

$$\mu(\lambda) = \alpha(\lambda) + i\beta(\lambda). \tag{F9}$$

It is very important to notice that, upon the varying parameter λ, the position and the stability of a stationary point can vary! For example, when λ passes some critical value λ_{crit} the real part of $\alpha(\lambda)$ may change sign and the stable equilibrium point may turn into an unstable point. This qualitative change of the equilibrium

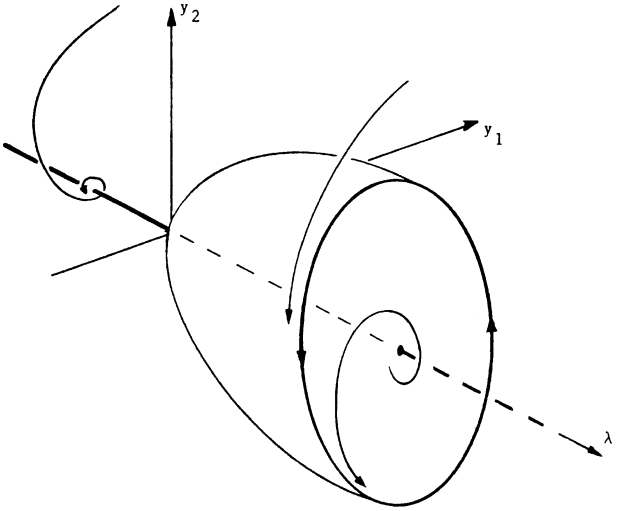

FIG. F1. Example of a Hopf bifurcation (see Seydel 1988). The limiting behavior from the trajectories near the equilibrium line change from a stable into a cyclic solution, when the critical value of a parameter λ_{crit} is passed (λ_{crit} is located at the intersect of the three axes).

solution when passing λ_{crit} is called branching or bifurcation. The type of bifurcation that connects a *stable* equilibrium with a periodic motion is called a Hopf bifurcation. In Fig. F1, taken from Seydel (1988), an example of a Hopf bifurcation is given. One sees the stable solution ''splits'' up in a cyclic solution when λ passes a certain value. The Jacobian evaluated at the Hopf bifurcation point has a pair of purely imaginary eigenvalues $\pm i\beta$, which denotes the beginning of a cycle. It can be shown that the existence of a Hopf bifurcation leads to two consequences:

1) the initial period (of zero amplitude at $(y_1^{eq}, y_2^{eq}, \lambda_{crit})$ is $2\pi/\beta$; and
2) the limit cycle has an amplitude proportional to $(\lambda - \lambda_{crit})^{1/2}$.

We mention that the validity of these statements close to the bifurcation points was verified for our system (not shown here).

REFERENCES

Beljaars, A. C. M., 1998: Role of the boundary layer in a numerical weather prediction model. *Clear and Cloudy Boundary Layers,* A. A. M. Holtslag, P. G. Duynkerke, and P. J. Jonker, Eds., Royal Netherlands Academy of Arts and Sciences, 287–304.

Blackadar, A. K., 1979: High-resolution models of planetary boundary layer. *Advances in Environmental Science and Engineering,* J. R. Pfafflin and E. N. Ziegler, Eds., Gordon and Breech, 50–85.

Businger, J. A., 1973: Turbulent transfer in the atmospheric surface layer. *Workshop on the Planetary Boundary Layer,* D. A. Haugen, Ed., Amer. Meteor. Soc., 67–98.

De Bruin, H. A. R., 1994: Analytic solutions of the equations governing the temperature fluctuation method. *Bound.-Layer Meteor.,* **68,** 427–432.

Derbyshire, S. H., 1999: Boundary-layer decoupling over cold surfaces as a physical boundary instability. *Bound.-Layer Meteor.,* **90,** 297–325.

Duynkerke, P. G., 1991: Observation of a quasi-periodic oscillation due to gravity waves in shallow radiation fog. *Quart. J. Roy. Meteor. Soc.,* **117,** 1207–1224.

Ha, K.-J., and Mahrt, L., 2001: Simple inclusion of *Z*-less turbulence within and above the modeled nocturnal boundary layer. *Mon. Wea. Rev.,* **129,** 2136–2143.

Holtslag, A. A. M., and F. T. M. Nieuwstadt, 1986: Scaling the atmospheric boundary layer. *Bound.-Layer Meteor.,* **36,** 201–209.

——, and H. A. R. De Bruin, 1988: Applied modelling of the nighttime surface energy balance over land. *Bound.-Layer Meteor.,* **27,** 689–704.

Hopf, E., 1942: Abzweigung einer periodischen Lösung von einer stationären Lösung eines Differentialsystems. *Bericht der Math.-Phys. Klasse der Sächsischen Akademie der Wissenschaften zu Leipzig,* Vol. 94, 1–22.

Hunt, J. C. R., J. C. Kaimal, and J. E. Gaynor, 1985: Some observations of turbulence structure in stable layers. *Quart. J. Roy. Meteor. Soc.,* **111,** 793–815.

Kondo, J., O. Kanechika, and N. Yasuda, 1978: Heat and momentum transfers under strong stability in the atmospheric surface layer. *J. Atmos. Sci.,* **35,** 1012–1021.

Lin, J. T., 1990: The effect of inertial and turbulence oscillations in the stable boundary layer and their role in horizontal dispersion. M.S. thesis, Dept. of Mathematics, University of Alabama in Huntsville, 82 pp.

Louis, J.-F., 1979: A parametric model of vertical eddy fluxes in the atmosphere. *Bound.-Layer Meteor.,* **17,** 187–202.

Mahrt, L., 1989: Intermittency of atmospheric turbulence. *J. Atmos. Sci.,* **46,** 79–95.

——, 1999: Stratified atmospheric boundary layers. *Bound.-Layer Meteor.,* **90,** 375–396.

——, J. Sun, W. Blumen, T. Delany, and S. Oncley, 1998: Nocturnal boundary layer regimes. *Bound.-Layer Meteor.,* **88,** 255–278.

Malhi, Y. S., 1995: The significance of the dual solutions for heat fluxes measured by the temperature fluctuation method in stable conditions. *Bound.-Layer Meteor.,* **74,** 389–396.

Marsden, J. E., and M. McCracken, 1976: *The Hopf Bifurcation and its Applications.* Springer, 408 pp.

McNider, R. T., D. E. England, M. J. Friedman, and X. Shi, 1995: Predictability of the stable atmospheric boundary layer. *J. Atmos. Sci.,* **52,** 1602–1614.

Nappo, C., 1991: Sporadic breakdown of stability in the PBL over simple and complex terrain. *Bound.-Layer Meteor.,* **54,** 69–87.

Nieuwstadt, F. T. M., and H. Tennekes, 1981: A rate equation for the nocturnal boundary-layer height. *J. Atmos. Sci.,* **38,** 1418–1428.

Poulos, G. S., D. C. Fritts, W. Blumen, and W. D. Bach, 2000: CASES-99 field experiment: An overview. Preprints, *14th Symp. on Boundary Layer and Turbulence,* Aspen, CO, Amer. Meteor. Soc., 618–621.

Revelle, D. O., 1993: Chaos and ''bursting'' in the planetary boundary layer. *J. Appl. Meteor.,* **32,** 1169–1180.

Seydel, R., 1988: *From Equilibrium to Chaos: Practical Bifurcation and Stability Analysis.* Elsevier, 367 pp.

Stull, R. B., 1983: Integral scales for the nocturnal boundary layer. Part I: Empirical depth relationships. *J. Climate Appl. Meteor.,* **22,** 673–686.

Turner, J. S., 1973: *Bouyancy Effects in Fluids.* Cambridge University Press, 368 pp.

Van de Wiel, B. J. H., R. J. Ronda, A. F. Moene, H. A. R. De Bruin, and A. A. M. Holtslag, 2002: Intermittent turbulence and oscillations in the stable boundary layer over land. Part I: A bulk model. *J. Atmos. Sci.,* **59,** 942–958.

Vukelic, B., and J. Cuxart, 2000: One-dimensional simulations of the stable boundary layer as observed in SABLES99. Preprints, *14th Symp. on Boundary Layer and Turbulence,* Aspen, CO, Amer. Meteor. Soc., 579–580.

Welch, R. M., M. G. Ravichandran, and S. K. Cox, 1986: Prediction of quasi-periodic oscillations in radiation fogs. Part I: Comparison of simple similarity approaches. *J. Atmos. Sci.,* **43,** 633–650.